Cancer Biol Med 2026. doi: 10.20892/j.issn.2095-3941.2025.0444

ORIGINAL ARTICLE

OPEN ACCESS

Mitochondrial uncoupling inhibits serine catabolism *via* FTO activation in metastatic breast cancer

Xin Jin[1,2]*, Albert M. Li[2,3]*, Man Zhao[2]*, Haowen Jiang[2], Yiren Xiao[2], Michaela Yip[2], Stavros Melemenidis[2], Scott Jackson[2], Yanan Yang[4], Cathyrin Simmermaker[4], Meng-Ning Zhou[2], Subarna Sinha[5], Daniel J. Cuthbertson[4], Erinn B. Rankin[2,3,6], Jiangbin Ye[2,3]

[1]Department of Oncology and Hematology, The Second Hospital of Jilin University, Changchun, Jilin 130000, China; [2]Department of Radiation Oncology, Stanford University School of Medicine, Stanford, CA 94305, USA; [3]Cancer Biology Program, Stanford University School of Medicine, Stanford, CA 94305, USA; [4]Agilent Technologies, Santa Clara, CA 95051, USA; [5]Department of Computer Science, Stanford University, Stanford, CA 94305, USA; [6]Department of Obstetrics and Gynecology, Stanford University, Stanford, CA 94305, USA

ABSTRACT

Objective: The mitochondrial serine catabolic pathway (MSCP) supports tumor proliferation and metastasis, yet no therapies target the MSCP. Because cancer cells rely on the MSCP when respiration is suppressed, we hypothesized that reactivating respiration would inhibit the MSCP.

Methods: Mitochondrial respiration was activated in triple negative breast cancer (TNBC) cells using uncouplers [niclosamide ethanolamine (NEN) and BAM15]. Metabolic activity through the MSCP was assessed using U-^{13}C-serine tracing and expression of key MSCP enzymes (SHMT2, MTHFD2, and MTHFD1L) were evaluated at the mRNA and protein levels. The NAD^+:NADH ratio and 2-hydroxyglutarate (2-HG) levels were determined using liquid chromatography-mass spectrometry. The role of m^6A RNA demethylase fat mass and obesity-associated protein (FTO) in regulating MSCP enzymes was examined using pharmacologic and genetic approaches. The therapeutic potential of mitochondrial uncoupling was tested *in vivo* using a lung metastasis model.

Results: Activation of mitochondrial respiration with NEN or BAM15 inhibited MSCP activity, as indicated by reduced labeling of glycine and purines from U-^{13}C-serine. Mitochondrial uncoupling markedly decreased the levels of SHMT2, MTHFD2, and MTHFD1L protein, despite unchanged or elevated mRNA levels. This post-transcriptional suppression was mediated by an increased NAD^+:NADH ratio, leading to reduced 2-HG production and subsequent activation of FTO. Inhibition of FTO, either pharmacologically or genetically, restored MSCP enzyme protein levels. Dietary mitochondrial uncoupling significantly suppressed lung metastasis *in vivo*.

Conclusions: The findings herein demonstrated that mitochondrial uncouplers inhibit MSCP through FTO-dependent m^6A demethylation. This work identified mitochondrial uncoupling as a novel and promising therapeutic approach for promoting m^6A demethylation and targeting MSCP in metastatic breast cancer.

KEYWORDS Mitochondria uncoupler; serine catabolism; one-carbon unit metabolism; FTO; m^6A; breast cancer; metastasis

Introduction

Serine catabolism, also referred to as the serine, glycine, and one-carbon (SG1C) metabolism pathway, is a metabolic process that generates amino acids, one-carbon units, and reducing equivalents necessary for cancer cell proliferation and survival[1,2]. In addition to contributing to phospholipid synthesis and cysteine production *via* the trans-sulfuration pathway, a key role of serine in cancer is the generation of one-carbon units and reducing equivalents in mitochondria[3-8]. Within mitochondria, serine is first converted to glycine by serine hydroxymethyltransferase 2 (SHMT2), concurrently producing 5,10-methylene-tetrahydrofolate (THF), which is oxidized to 10-formyl-THF by methylene-tetrahydrofolate

*These authors contributed equally to this work.
Correspondence to: Erinn B. Rankin and Jiangbin Ye
E-mail: erankin@stanford.edu and jiangbinye@muhn.edu.cn
ORCID ID: https://orcid.org/0000-0002-2045-2296 and https://orcid.org/0000-0003-1117-4869
Received August 26, 2025; accepted January 28, 2026;
published online March 12, 2026.
Available at www.cancerbiomed.org
©2026 The Authors. Creative Commons Attribution-NonCommercial 4.0 International License (CC BY-NC 4.0)

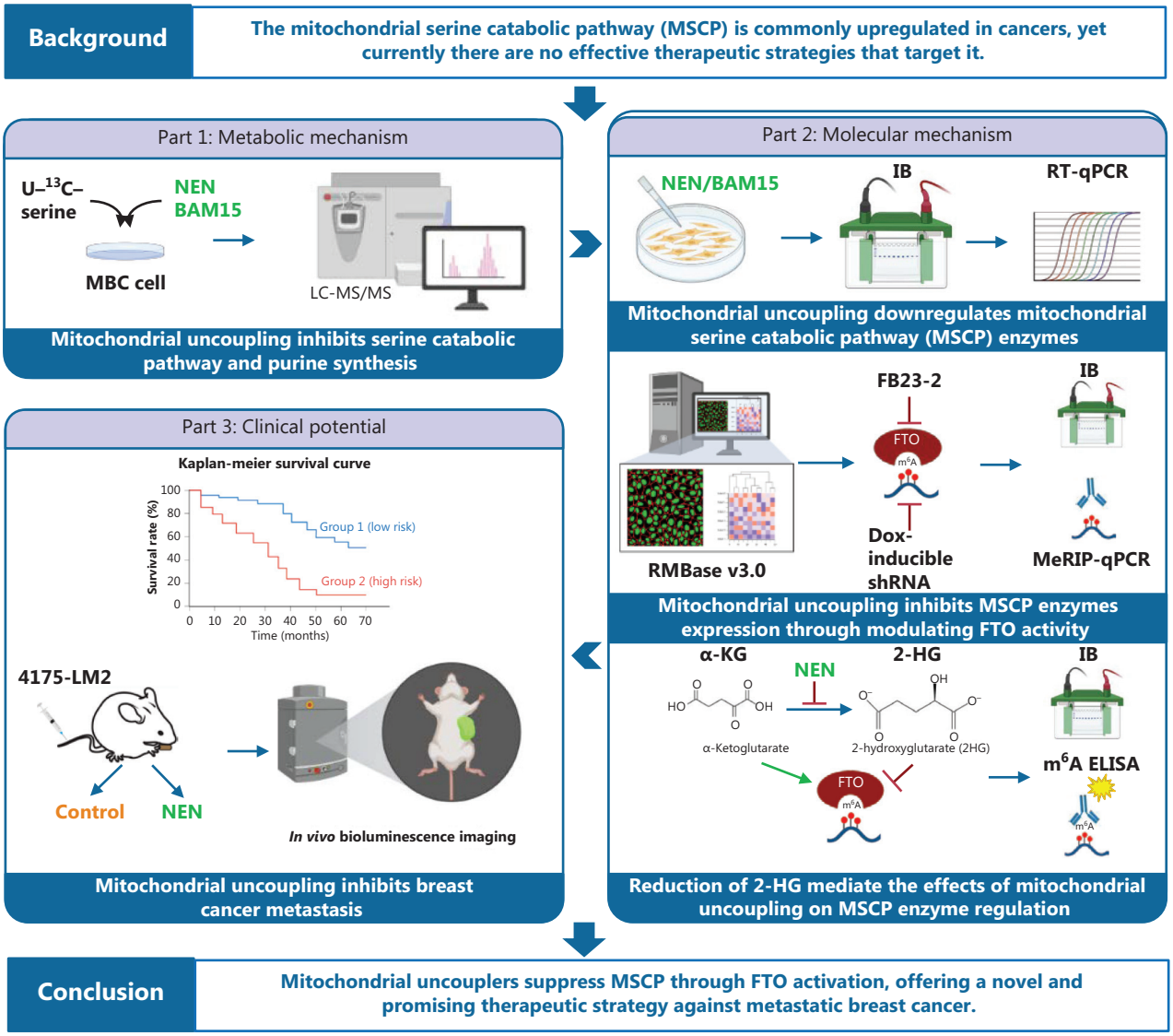

Study Flowchart The study was structured in three parts to systematically investigate the therapeutic potential of mitochondrial uncoupling in metastatic breast cancer. Part I used a U-^{13}C-serine tracing approach, which revealed that mitochondrial uncoupling suppresses the MSCP. Part II delineated the underlying mechanism, combining bioinformatic analysis, immunoblotting, MeRIP-qPCR, and ELISA to demonstrate that mitochondrial uncoupling downregulates key MSCP enzymes *via* FTO-dependent RNA demethylation. Part III evaluated the clinical relevance of FTO expression as a prognostic biomarker and explored the therapeutic efficacy of mitochondrial uncouplers in metastatic breast cancer models. Collectively, this work established mitochondrial uncoupling as a novel strategy to promote m^{6}A demethylation and inhibit the MSCP, offering a promising therapeutic avenue for metastatic breast cancer. MSCP, mitochondrial serine catabolic pathway; MBC, metastatic breast cancer; NEN, niclosamide ethanolamine; LC-MS, liquid chromatography-mass spectrometry; IB, immunoblotting; RT-qPCR, reverse transcription-quantitative polymerase chain reaction; FTO, fat mass and obesity-associated protein; MeRIP, methylated RNA immunoprecipitation; ELISA, enzyme-linked immunosorbent assay.

dehydrogenase 2 (MTHFD2) and 2-like (MTHFD2L). The 10-formyl-THF is further oxidized by methylenetetrahydrofolate dehydrogenase 1-like (MTHFD1L) to form formate, which can exit the mitochondria[2,6,9]. The reductive environment in the cytosol created by NADPH-generating pathways, such as the pentose phosphate pathway (PPP)[10], facilitates the reduction of formate *via* MTHFD1 to regenerate 10-formyl-THF, a one-carbon unit essential for *de novo* purine biosynthesis.

Upregulation of the mitochondrial serine catabolic pathway (MSCP) is a well-established metabolic hallmark of cancer. Among metabolic enzymes, SHMT2 and MTHFD2 are

consistently among the most upregulated enzymes in human cancers[11,12], while the cytosolic isoform (SHMT1) is typically downregulated in cancer[12]. This differential regulation (upregulation of SHMT2 and downregulation of SHMT1) correlates with poor prognosis in breast cancer patients[13].

Upregulation of MSCP in cancer represents an adaptive response to electron transport chain (ETC) inhibition. SHMT2, a direct target of hypoxia-inducible factor 1-alpha (HIF-1α), is induced under hypoxic conditions, especially in cells with elevated Myc activity[13]. In addition, among NAD^+-dependent mitochondrial catabolic pathways, MSCP is uniquely resistant to ETC inhibition, largely due to the high tolerance of MTHFD2 to high NADH levels[14]. Consequently, cancer cells preferentially rely on MSCP to generate reducing equivalents, such as NADH and NADPH, which are essential for maintaining redox homeostasis under conditions of impaired ETC activity[5,12,14].

Despite the significance of the MSCP in cancer progression, there are currently no effective therapeutic strategies that target the MSCP. In this study pharmacologic activation of mitochondrial respiration through uncouplers was shown to suppress MSCP activity in metastatic breast cancer cells. Mitochondrial uncoupling increased the cellular NAD^+:NADH ratio and reduced 2-hydroxyglutarate (2-HG) levels, leading to post-transcriptional downregulation of key MSCP enzymes through the m^6A RNA demethylase fat mass and obesity-associated protein (FTO). These findings uncover a previously unrecognized mechanism connecting m^6A methylation to regulation of serine metabolism and suggest mitochondrial uncoupling as a potential therapeutic approach to inhibit MSCP-dependent tumor progression.

Materials and methods

Cell lines

4175-LM2 and MDA-MB-468 cells were obtained from Dr. Joan Massagué (Memorial Sloan-Kettering Cancer Center, New York City, NY, USA). The 4175-LM2 cell line is a metastatic subclone of MDA-MB-231 that was previously isolated through *in vivo* selection due to a high metastasis rate and specific tropism for the lung[15]. The 4175-LM2 cell line also expresses luciferase, making 4175-LM2 cells ideal for monitoring metastasis *in vivo*. MiaPaCa-2 and Panc-1 cells were obtained from Dr. Laura Attardi (Stanford University, Palo Alto, CA, USA). All cells were cultured in DMEM/F12 with 10% fetal bovine serum (Sigma, St. Louis, MO, USA) with 1% penicillin/streptomycin. All cell lines were tested every 3–6 months and were negative for mycoplasma (MycoAlert Mycoplasma Detection Kit; Lonza Bioscience, Walkersville, MD, USA). These cell lines were not authenticated by the authors. All cell lines used in experiments were passed ≤ 10 times from the time of thawing.

Metabolite profiling and mass spectrometry

For U-^{13}C-serine labeling experiments, Parental and metastatic cells were cultured in RPMI-1640 medium lacking glucose, serine, and glycine (TEKnova; Hollister, CA, USA) and supplemented with 2 g/L glucose and 0.03 g/L U-^{13}C-serine serine (Cambridge Isotope Laboratories; Tewksbury, MA, USA) for U-^{13}C-serine labeling experiments with or without uncouplers for up to 24 h before harvesting. Cells were washed twice with ice-cold PBS prior to extraction with 400 μL of acetonitrile:water (80:20) over ice for 15 min. Cells were scraped off plates to be collected with supernatants, sonicated for 30 s, then spun down at 1.5×10^4 rpm (18,000 *g*) for 10 min. The supernatant (200 μL) was removed immediately for liquid chromatography- mass spectrometry (LC-MS/MS) analysis.

Quantitative LC-electrospray ionization (ESI)-MS analysis of U-^{13}C-serine-labeled cell extracts was performed using an Agilent Technologies 1290 UHPLC system equipped with an Agilent Technologies 6545 LC/quadrupole time-of-flight (QTOF) mass spectrometer (Santa Clara, CA, US). A hydrophilic interaction chromatography method (HILIC) with a BEH amide column (100 × 2.1 mm i.d., 1.7 μm; Waters, Milford, MA, USA) was used for compound separation at 35°C (column oven temperature) with a flow rate of 0.3 mL/min. Mobile phase A consisted of 25 mM ammonium acetate and 25 mM ammonium hydroxide in water and mobile phase B was acetonitrile. The gradient elution was as follows: 0–1 min, 85% B; 1–12 min, 85% B → 65% B; 12–12.2 min, 65% B-40% B; and 12.2–15 min, 40% B. The column was re-equilibrated at 85% B for 5 min after the gradient. The overall runtime was 20 min and the injection volume was 5 μL. An Agilent Q-TOF 6545 mass spectrometer equipped with a Dual AJS ESI source was operated in the negative ion mode. The ion source settings were as follows: capillary voltage (VCap), 3500 V; fragmentor, 125 V; skimmer, 65 V; Oct 1 RF, 750 V; drying gas, 11 L/min at 300°C; nebulizer, 40 psi; and sheath gas, 11 L/min at 320°C. A full scan range was set at 50–1600 (m/z). Continuous mass-axis calibration was performed using reference ions at 119.0363 and 980.0164 m/z. Isotopologue extraction was performed in Agilent Technologies MassHunter Profinder B.08.00. The retention time (RT) of each metabolite was determined by authentic standards. The mass tolerance was set to ±15 ppm and the RT tolerance was ±0.2 min. Natural isotope abundance was corrected using Agilent Technologies MassHunter Profinder software.

Seahorse assay

A total of 30,000 cells/well were seeded into Seahorse 96 well microplates, incubated overnight, then subjected to continuous oxygen consumption rate (OCR) measurements over 6 h using Agilent Seahorse XFe96 analyzer, during which the indicated compounds or vehicle control were injected through

port A at the start of the assay. The complex I inhibitor (rotenone) and complex III inhibitor (antimycin A) were used as negative controls. All OCR values were normalized to baseline measurements.

RNA interference (RNAi)

Doxycycline (Dox)-inducible FTO knockdown short hairpin (sh)RNA-expressing virus was obtained using a previously published method[16]. Pooled populations were tested for on-target knockdown by immunoblot. Cells were first treated with Dox for 24 h, followed by niclosamide ethanolamine (NEN) treatment for 48 h with Dox. shCtrl: 5′-GCAGGTCTGAAGTTCAT-3′; shFTO: 5′-TCACCAAGGAGACTGCTATTT-3′

Immunoblot

The following antibodies were used: anti-SHMT1 (HPA078682; Sigma); anti-SHMT2 (HPA020543; Sigma); anti-MTHFD2 (41377S; Cell Signaling, Danvers, MA, USA); anti-MTHFD1L (14998S; Cell Signaling); anti-FTO (D2V1I; Cell Signaling); and anti-β-actin (3700S; Cell Signaling).

RNA isolation, reverse transcription, and real-time PCR

Total RNA was isolated from tissue culture plates according to the TRIzol reagant protocol (Invitrogen; Carlsbad, CA, USA). Total RNA (3 μg) was used in the reverse transcription reaction according to the SuperScript III protocol (Invitrogen). Quantitative PCR amplification was performed on the Prism 7900 Sequence Detection System (Applied Biosystems, Waltham, MA, USA) using Taqman Gene Expression Assays (Applied Biosystems). Gene expression data were normalized to 18S rRNA.

m^{6}A RNA methylation quantification

RNA concentration was measured using NanoDrop 2000 (Thermo Scientific, Waltham, MA, USA). Global m^{6}A levels were determined with an EpiQuiK™ m^{6}A RNA Methylation Quantification Kit (P-9005-96; EpiGentek, Farmingdale, NY, USA), according to the manufacturer's instructions. Briefly, 200 ng of total RNA per sample was used for m^{6}A measurement. The percentage of m^{6}A in the total RNA was calculated using the following formula:

$$\mathrm{m^6A\,\%} = \frac{(\mathrm{Sample\,OD} - \mathrm{NC\,OD}) \div \mathrm{S}}{(\mathrm{PC\,OD} - \mathrm{NC\,OD}) \div \mathrm{P}} \times 100\%$$

Where NC is the negative control, PC is the positive control, S is the amount of input sample RNA in ng, and P is the amount of input PC in ng.

MeRIP-qPCR

Input and IP BAM files were obtained for 4 breast cancer cell lines (4175-LM2, MDA-MB231, MCF7, and SKBR3) from the Gene Expression Omnibus [GEO (GSE137258)] to identify m^{6}A peaks in MSCP mRNAs[17]. Uniquely mapped reads were subjected to peak-calling analysis using MACS2 (v 2.2.9.1) software with the following parameters:

macs2 callpeak -t IP.bam -c Input.bam -f BAM -g hs --nomodel --extsize 50 -q 0.05.

Peaks overlapping with exons (5′UTR and 3′UTR) were identified in the genes of interest (*SHMT1*, *SHMT2*, *MTHFD1L*, and *MTHFD2*). IGV visualization software was used to visualize the m^{6}A peaks. The replicates of each cell line were averaged using deepTools, then visualized.

m^{6}A RNA immunoprecipitation was performed with the EpiQuik™ CUT&RUN m^{6}A RNA Enrichment (MeRIP) Kit (P-9018; Epigentek, Farmingdale, NY, USA). Briefly, 200–500 ng of total RNA was incubated with the magnetic bead–conjugated anti-m^{6}A antibody provided in the MeRIP Kit under optimized binding conditions. m^{6}A-enriched RNA was eluted and purified according to the manufacturer's instructions after sequential washes to remove non-specific RNA. A fraction of total RNA was reserved as input control.

Eluted RNA and corresponding input RNA were reverse-transcribed using the High-Capacity cDNA Reverse Transcription Kit (Applied Biosystems). qPCR was performed using SYBR Green Master Mix (Bio-Rad, Hercules, CA, USA) on a QuantStudio real-time PCR system (Waltham, MA, USA). m^{6}A enrichment was calculated using the percent-input method. The following primer pairs were used for qPCR: SHMT2 exon 1 (forward, TTGCTGCCCTAGACCAGAGT; and reverse, CGAGCCGCCCAAAACAAAGA); and MTHFD1L 3′UTR (forward, GTGGACAAGGCTCTCACAGG; and reverse, CCAACTGCAGCAAAAAGGCA).

In vivo tumor metastasis assay

All procedures involving animals and their care were approved by the Institutional Animal Care and Use Committee of Stanford University in accordance with institutional and National Institutes of Health guidelines (Protocol Approval No. APLAC-32251).

Cells (0.2×10^5 4175-LM) were injected *via* tail vein into 6–8-week-old female NOD SCID mice for the lung metastasis assay. Mice were imaged weekly using the Xenogen IVIS 200 (PerkinElmer, Waltham, MA, USA). Briefly, mice were injected intraperitoneally with 100 μg/g of D-luciferin (potassium salt; PerkinElmer) on the day of imaging. The mice were anesthetized in an anesthesia-induction chamber 8 min later using a mixture of 3% isoflurane (Fluriso; VetOne, Boise, ID, USA) in O_2. Anesthesia was maintained with a mixture of 2% isoflurane in O_2 inside the imaging chamber. Images were

acquired (exposure time, auto; F stop. 1.2; binning, medium) using Living Image (PerkinElmer) from the dorsal and ventral aspects of mice. The total photon flux (p/sec/cm^2/sr) per animal was calculated by averaging the signal acquired from the dorsal and ventral aspects.

Lungs were harvested from 17 mice (8 control and 9 NEN-treated) at the experimental endpoint, perfused with PBS, snap-frozen in liquid nitrogen, and stored at −80°C. Total RNA was extracted from individual lung lobes (~20–30 mg) using the EpiQuik Total RNA Isolation Kit (P-9100; Epigentek) according to the manufacturer's instructions. Species-specific primers targeting human GAPDH-to-mouse 18S rRNA were used to quantify human tumor content relative to mouse tissue. The relative human tumor burden in each lung was calculated as the ratio of human GAPDH-to-mouse 18S rRNA. Group comparisons were performed using an unpaired two-tailed Student's *t*-test. The data are presented as the mean ± SEM. A $P < 0.05$ was considered statistically significant.

Patient survival analysis

Kaplan–Meier analysis was performed using R2 [Genomics Analysis and Visualization Platform (http://r2.amc.nl)]. The dataset were GSE42568[18] and GSE31448[19].

Statistical analysis

The results are presented as the mean ± SD or mean ± SEM depending on the assay type, as detailed in the figure legends. Statistical comparisons between groups were performed using Student's *t*-test or one- or two-way ANOVA (two-tailed, assuming unequal variance). A *P*-value < 0.05 was considered statistically significant. Relapse-free survival was analyzed using the Kaplan–Meier method.

Results

Mitochondrial uncoupling inhibits serine catabolic pathway and purine synthesis

We hypothesized that activating ETC and mitochondrial respiration with uncouplers would suppress serine catabolism given that activation of serine catabolism is an adaptive response to ETC inhibition[12,14]. To test this hypothesis isotope tracing was performed using U-^{13}C-serine (**Figure 1A**). Treatment with the mitochondrial uncouplers, NEN[20] and BAM15[21], for 2 or 24 h did not alter the m + 3 labeling of serine, indicating that uncoupling does not impact serine uptake (**Figures 1B,1C,S1A and S1B**). However, uncoupler treatment significantly reduced m + 2 labeled glycine in the triple-negative breast cancer (TNBC) cell lines, 4175-LM2 (a lung-metastatic subclone of MDA-MB-231)[13,15] and MDA-MB-468. Furthermore, prolonged treatment (24 h) resulted in a marked decrease in purine nucleotide labeling (m + 4 ATP and m + 4 GTP; **Figures 1B,1C, and S1B**), which incorporated four labeled carbons derived from one glycine molecular and two one-carbon units (**Figure 1A**). As a mitochondrial uncoupler, NEN treatment increased the OCR in these cell lines (**Figure 1D**). NEN also elevated the NAD^+:NADH ratio, indicating the activation of complex I (**Figure 1E**)[22,23]. These findings demonstrated that mitochondrial uncoupling effectively activates ETC respiration in these TNBC cells and inhibits serine catabolism and *de novo* purine biosynthesis. In addition, NEN and BAM15 induced significant, dose-dependent proliferation arrest with IC_{50} values of 0.8259 μM for NEN and 8.212 μM for BAM15 in 4175-LM2 cells (**Figure S1C**).

Mitochondrial uncoupling downregulates MSCP enzymes

The expression of MSCP enzymes (especially SHMT2 and MTHFD2) are markedly upregulated in various cancer types[11]. We previously identified *SHMT2* as a hypoxia-inducible gene, suggesting that the increased expression of these enzymes are an adaptive response to ETC inhibition[12]. This led us to determine if ETC activation *via* an uncoupler modulates MSCP enzyme expression.

Strikingly, prolonged treatment with the mitochondrial uncouplers, NEN or BAM15, significantly downregulated the expression of SHMT2, MTHFD2, and MTHFD1L in 4175-LM2 and MDA-MB-468 cells, while the cytosolic enzyme, SHMT1, remained unaffected (**Figures 2A and S2A**). Similar downregulation of MSCP enzymes was observed in the pancreatic cancer cell lines, MiaPaCa-2 and Panc-1, following uncoupler treatment (**Figure S2B**), indicating the inhibitory effect of uncoupling on MSCP enzymes is not limited to breast cancer cells. SHMT2 is known to be transcriptionally regulated by Myc[24,25] and is induced by HIF-1 under hypoxic conditions[12]. These findings prompted us to determine if downregulation of MSCP enzymes following uncoupler treatment occurred at the transcriptional level. Surprisingly, NEN or BAM15 treatment did not decrease the levels of SHMT2, MTHFD2, or MTHFD1L mRNA. In fact, mRNA levels of these genes were upregulated at 24 h time points (**Figures 2B and S2C**). These results suggested that uncouplers reduce MSCP enzyme expression *via* post-transcriptional mechanisms rather than transcriptional repression.

Mitochondrial uncoupling inhibits MSCP enzyme expression by modulating FTO activity

The observation that MSCP enzymes are downregulated upon mitochondrial uncoupling likely occurs at the

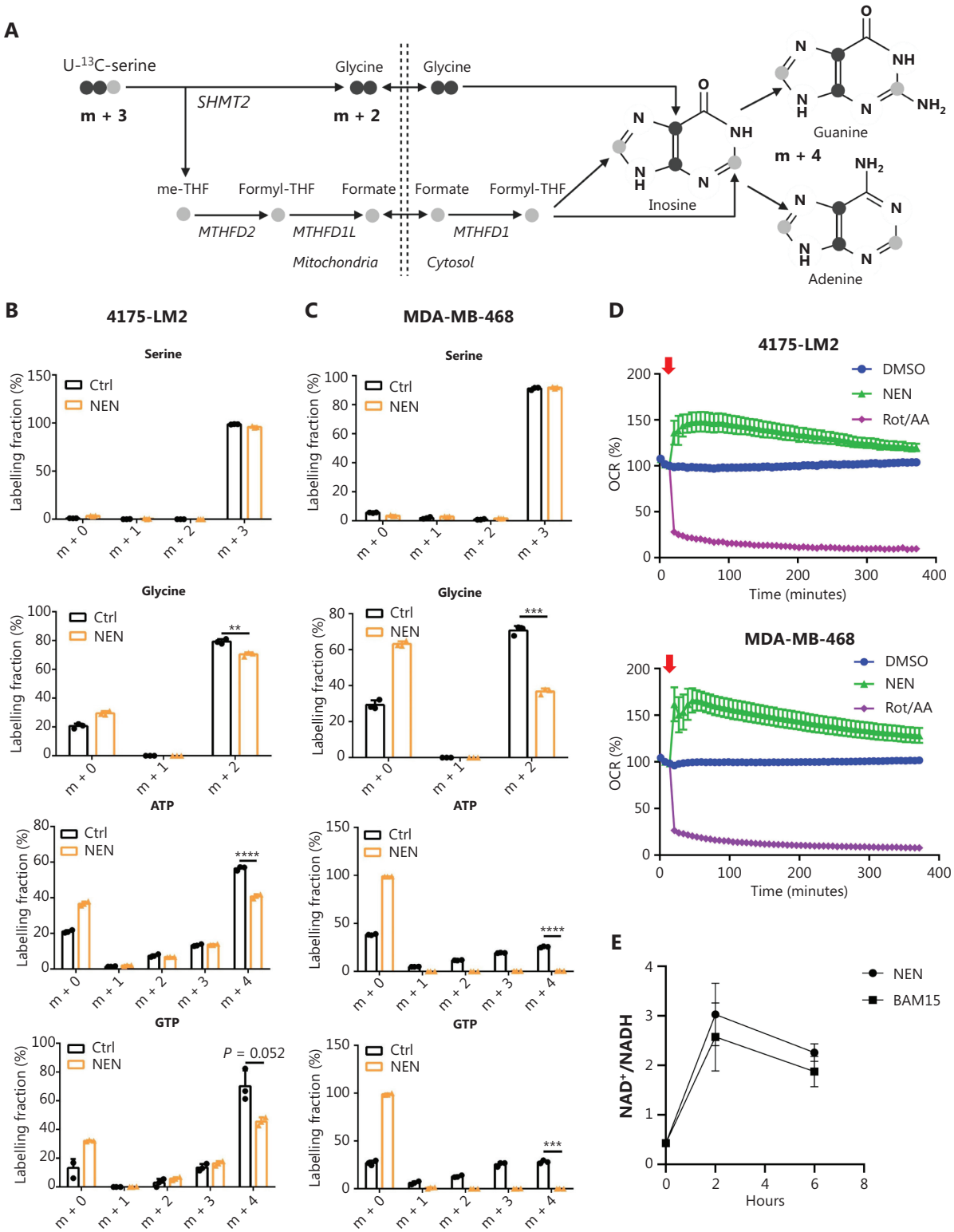

Figure 1 Mitochondrial uncoupling inhibits serine catabolism and *de novo* purine synthesis. (A) A schematic of the SCP pathway with U-^{13}C-serine tracing. The dark cycle indicates ^{13}C labeling in glycine, while the light cycle represents ^{13}C labeling in one-carbon units. (B and C) 4175-LM2 and MDA-MB-468 cells were treated with DMSO control or 1 μM NEN and labeled with U-^{13}C-serine for 24 h. The isotope labeling fractions of metabolites were measured using LC-MS (mean ± SD, n = 3, $^{**}P < 0.01$ $^{***}P < 0.001$ $^{****}P < 0.0001$ by two-tailed

Student's *t*-test). (D) 4175-LM2 and MDA-MB-468 cells were treated with DMSO control, 1 μM NEN, or 1 μM rotenone + antimycin A (Rot/AA). The oxygen consumption rate (OCR) was measured continuously on Seahorse XF Analyzer (n = 4). Red arrow indicates when treatment started. (E) 4175-LM2 cells were treated with 1 μM NEN or 10 μM BAM15 for the indicated times and the NAD^+:NADH ratio was determined by LC-MS (mean ± SD, n = 3).

post-transcriptional level prompted us to identify the potential regulators. The expression of RNA modification-related proteins was examined in breast cancer tissues and compared to normal breast tissues using RMBase v3.0[26] (**Figure 3A**). Several RNA modifiers that are involved in N6-adenosine-methylation (m^6A), the most abundant modification on eukaryotic mRNA, were significantly downregulated in breast cancer, including the following: components of the m^6A methyltransferase complex [methyltransferase 14, N6-adenosine-methyltransferase non-catalytic subunit (METTL14)], which is essential for RNA-binding, substrate recognition, and complex stability[27,28], Wilms tumor 1-associated protein (WTAP), an adaptor protein that localizes the METTL3-METTL14 complex to nuclear speckles[29,30], zinc finger CCCH-type containing 13 (ZC3H13), a scaffold protein that anchors the m^6A methyltransferase complex in the nucleus[31], and methyltransferase 16, RNA N6-adenosine (METTL16), a standalone methyltransferase that only methylates a specific set of targets, including MAT2A mRNA and U6 snRNA[32-34]; and FTO, the first discovered m^6A demethylase[35]. The expression of m^6A reader proteins [insulin-like growth factor 2 mRNA-binding protein 1 (IGF2BP1) and insulin-like growth factor 2 mRNA-binding protein 2 (IGF2BP2)][36] are differentially regulated in breast cancer with IGF2BP1 upregulated and IGF2BP2 downregulated. Together, these findings suggested dysregulation of m^6A RNA modifications in breast cancer.

RNA N6-methyladenosine (m^6A) modification is the most abundant epi-transcriptomic mark on RNA with a key role regulating RNA splicing, translation, and stability[37,38]. Recent studies have suggested that dysregulation of the m^6A epi-transcriptome is a common feature of tumorigenesis[39]. However, the role of the m^6A demethylase FTO[35] appears to be complex and context-dependent. FTO is overexpressed and has been identified as a synthetic lethal target with VHL in clear cell renal cell carcinoma (ccRCC)[16], likely because FTO promotes glutamine metabolism through upregulation of solute carrier family 1 member 5 (SLC1A5)[40]. In contrast, FTO is consistently repressed across all breast cancer subtypes (**Figures 3B and S3A**). The other known m^6A demethylase, [AlkB homolog 5 (ALKBH5)][41], is significantly downregulated in HER2-positive breast cancer but not in luminal or TNBC subtypes (**Figures 3B and S3A**). These findings suggested that, unlike an oncogenic role in ccRCC, FTO may function as a tumor suppressor in breast cancer.

The effects of both pharmacologic and genetic inhibition of FTO on MSCP enzyme levels following NEN treatment were examined to investigate whether FTO regulates MSCP enzyme expression. Interestingly, treatment with the FTO inhibitor, FB23-2, restored the expression of the MSCP enzymes (SHMT2, MTHFD2, and MTHFD1L) that was lost upon mitochondrial uncoupling (**Figure 3C**). In addition, knockdown of FTO using a Dox-inducible shRNA system (**Figure S3B**)[16] partially rescued the expression of MTHFD2 and MTHFD1L upon uncoupling. However, SHMT2 expression was not restored, likely due to incomplete FTO knockdown (**Figure 3D**).

By analyzing existing m^6A sequencing dataset from breast cancer cell lines[17], m^6A methylation peaks, indicating site-specific RNA modification, were found in the first exon of the *SHMT2* transcript and the 3′ untranslated region (3′UTR) of *MTHFD1L* (**Figure S3C**). Methylated RNA immunoprecipitation (MeRIP)-qPCR analysis was performed in 4175-LM2 cells following knockdown of FTO. The increase in m^6A peaks at exon I of *SHMT2* and the 3′UTR of *MTHFD1L* following FTO knockdown indicated that these are direct regulatory targets of the FTO demethylase (**Figure 3E**). Downregulation of MSCP mRNAs following FTO knockdown (**Figure S3D**), which is consistent with upregulation by mitochondrial uncouplers (**Figure 2B**), further validated that FTO downregulates MSCP protein levels through post-transcriptional regulation. Collectively, these data suggested that FTO is a key negative regulator of MSCP enzyme expression upon mitochondrial uncoupling.

Reduction of 2-HG mediates the effects of mitochondrial uncoupling on MSCP enzyme regulation

Next, the potential mechanism by which FTO is required for downregulation of MSCP enzymes following mitochondrial uncoupling was examined. Like the DNA demethylase, ten-eleven translocation (TET), the m^6A RNA demethylase FTO is an α-ketoglutarate (α-KG)-dependent dioxygenase that uses α-KG as a substrate and can be inhibited by D-2-hydroxyglutarate (D-2-HG), which is produced from the mutant isocitrate dehydrogenase (mIDH) enzyme in leukemia[42], as well as L-2-hydroxyglutarate (L-2-HG)[42]. Over-expression of L-2-hydroxyglutarate dehydrogenase (L2HGDH) reduced global m^6A levels in kidney cancer cells[43]. Unlike leukemia cells, breast cancer cells rarely carry IDH mutations. However, leukemia cells often exhibit comparably

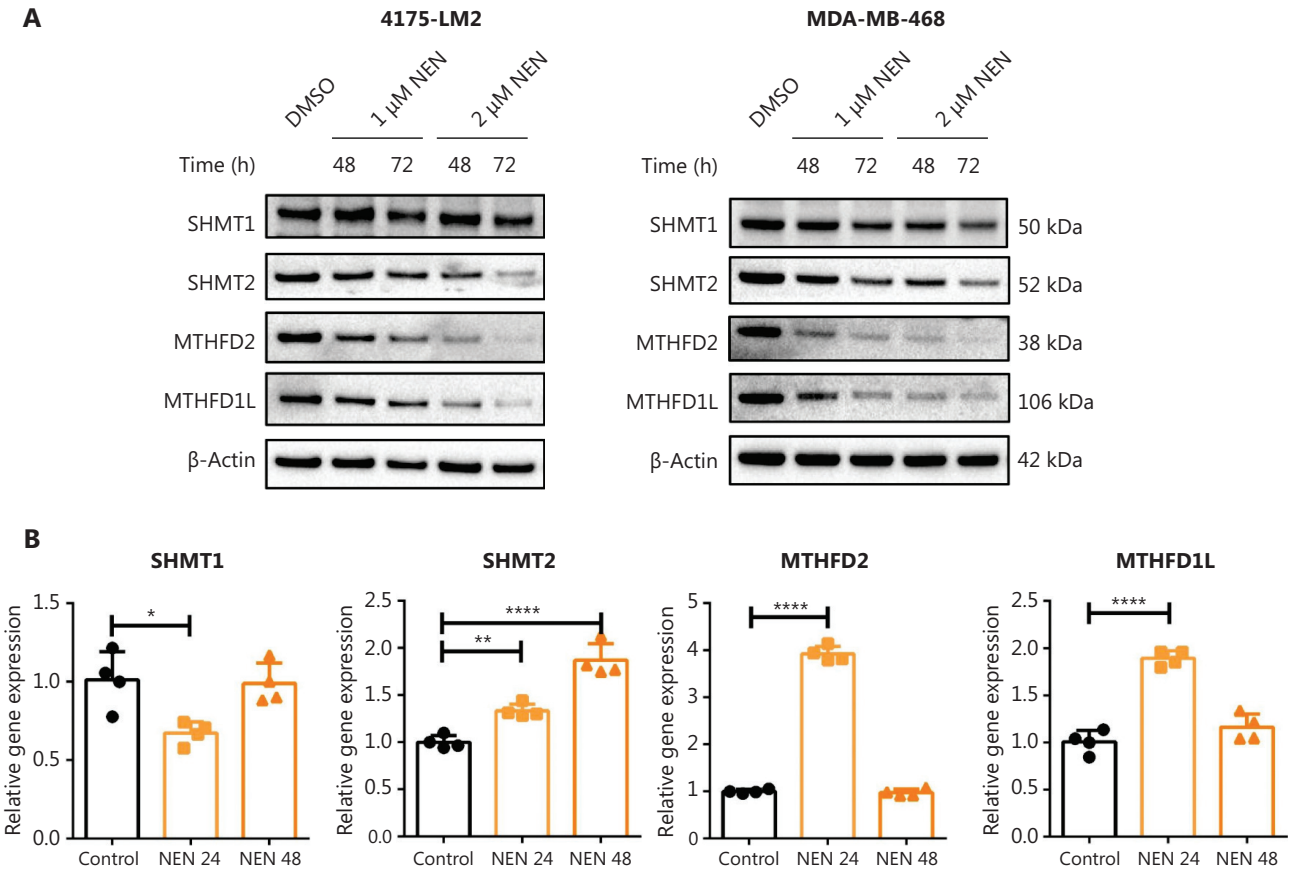

Figure 2 Mitochondrial uncoupling downregulates mitochondrial serine catabolic pathway (MSCP) enzymes. (A) Immunoblots of the MSCP enzymes in 4175-LM2 and MDA-MB-468 cells treated with different concentrations of NEN for 48 or 72 h. (B) RT-qPCR analysis of *SCP* gene expression in 4175-LM2 cells treated with 1 μM NEN for 24 or 48 h (mean ± SD, $n = 4$, *$P < 0.05$ **$P < 0.01$ ***$P < 0.001$ ****$P < 0.0001$ by two-tailed Student's *t*-test).

high levels of 2-HG, particularly in estrogen receptor (ER)-negative and basal-like subtypes[44]. Breast cancer cells contain D-2-HG and L-2-HG with L-2-HG being predominantly enriched in ER-negative subtypes[45]. Under conditions of ETC inhibition, such as hypoxia, L-2-HG is primarily generated *via* the NADH-dependent reduction of α-KG[46,47]. In addition, 3-phosphoglycerate dehydrogenase (PHGDH), the first enzyme in the serine biosynthetic pathway, can catalyze NADH-dependent reduction of α-KG to D-2-HG[48,49]. Therefore, high NADH is likely to be the driver of 2-HG production in cells without mIDH. We previously discovered that NEN treatment increases the NAD^+:NADH ratio, impairs 2-HG production, and decreases DNA promoter CpG island methylation to promote differentiation in neuroblastoma[22]. Based on these findings, we hypothesized that NEN treatment may similarly decrease m^6A RNA methylation levels by downregulating 2-HG levels. NEN treatment significantly reduced 2-HG levels in 4175-LM2 cells (**Figure 4A**), which was associated with a corresponding decrease in m^6A levels (**Figure 4B**) and consistent with our previous observations in neuroblastoma cells. Supplementing the culture media with cell-permeable octyl-L-2-HG increased m^6A levels, while treatment with cell-permeable dimethyl-α-KG decreased m^6A levels (**Figure 4C**), which is consistent with the reciprocal functions of these two metabolites on α-KG-dependent dioxygenases, further suggesting that 2-HG levels are a key determinant of m^6A methylation levels. Of note, octyl-L-2-HG treatment upregulated the expression of MSCP enzymes, as well as SHMT1 (**Figure 4D**), while dimethyl-α-KG treatment reduced the expression of MTHFD2 and MTHFD1L (**Figure 4E**). Collectively, these data suggested that downregulation of 2-HG and m^6A is a key mechanism by which mitochondrial uncouplers suppress MSCP enzyme expression.

Mitochondrial uncoupling inhibits breast cancer metastasis

We previously reported that MSCP enzymes are highly expressed in late-stage breast cancer and metastatic cell lines[13].

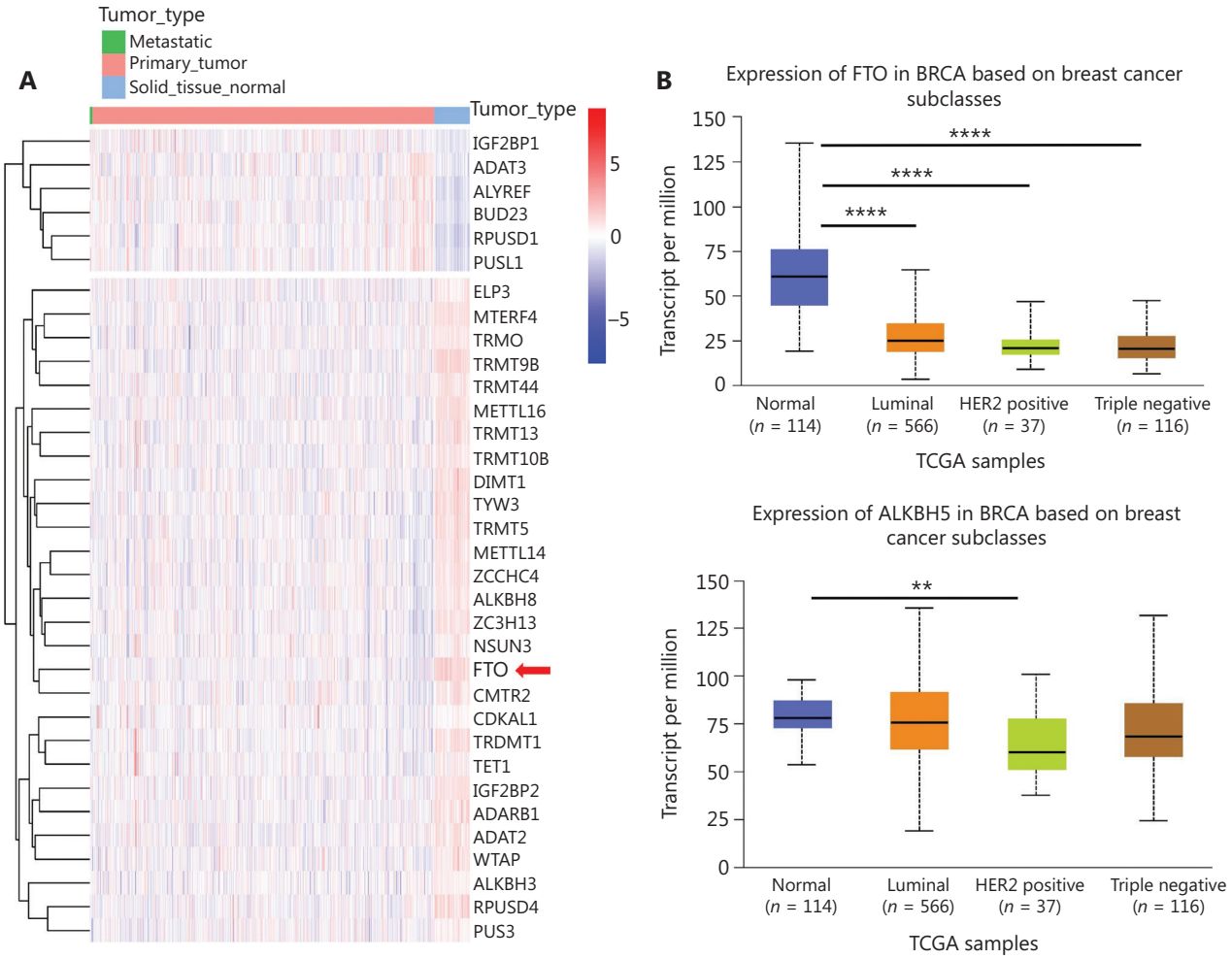

Figure 3 Continued

Notably, low FTO expression is associated with poorer relapse-free survival in breast cancer patients (GSE42568[18] and GSE31448[19]; **Figure 5A and B**). Multivariate Cox proportional hazards analyses were also performed to assess whether FTO serves as an independent prognostic factor. FTO, grade, and ER status were adjusted for in GSE42568. ER status was stratified due to violation of the proportional hazards assumption in GSE31448. Specifically, the effect of ER positivity varied over time with the beneficial effect observed primarily during early follow-up, so only FTO and grade were adjusted. Higher grade was significantly associated with an increased risk of relapse or death in both models, whereas FTO expression was not a significant prognostic factor ($P = 0.222$ and $P = 0.056$, respectively; **Figure S4A**). These findings suggested that FTO tumor suppressor activity in breast cancer may vary with tumor grade and molecular subtype.

Expression data using MammOnc-DB was analyzed to determine whether FTO is also differentially expressed in metastatic *vs.* primary tumors[50]. FTO expression was shown to be further downregulated in metastases to the lung, liver, and other sites relative to primary tumors, although the differences were not statistically significant and likely due to the limited sample size (**Figures 5C and S4B**). In contrast, SHMT2 was significantly overexpressed in all metastatic samples (**Figures 5C and S4B**), while no such associations were demonstrated for MTHFD2 and MTHFD1L (**Figure S4C**). Combined with our previous findings that SHMT2 inhibition can reduce breast cancer metastasis, these data suggested that FTO downregulation may be particularly detrimental in patients with metastatic disease[13], in which SHMT2 is overexpressed.

A model of breast cancer lung metastasis[13,15] using luciferase-expressing 4175-LM2 cells was adopted to evaluate the therapeutic potential of mitochondrial uncoupling in treating metastatic breast cancer. Mice fed a diet containing 2000 ppm NEN, a dose considered tolerable and safe[20,22,51], exhibited a significant reduction in lung metastasis, as demonstrated by *in vivo* bioluminescence imaging (**Figure 6A and B**) and confirmed by endpoint qPCR analysis of the lung metastasis

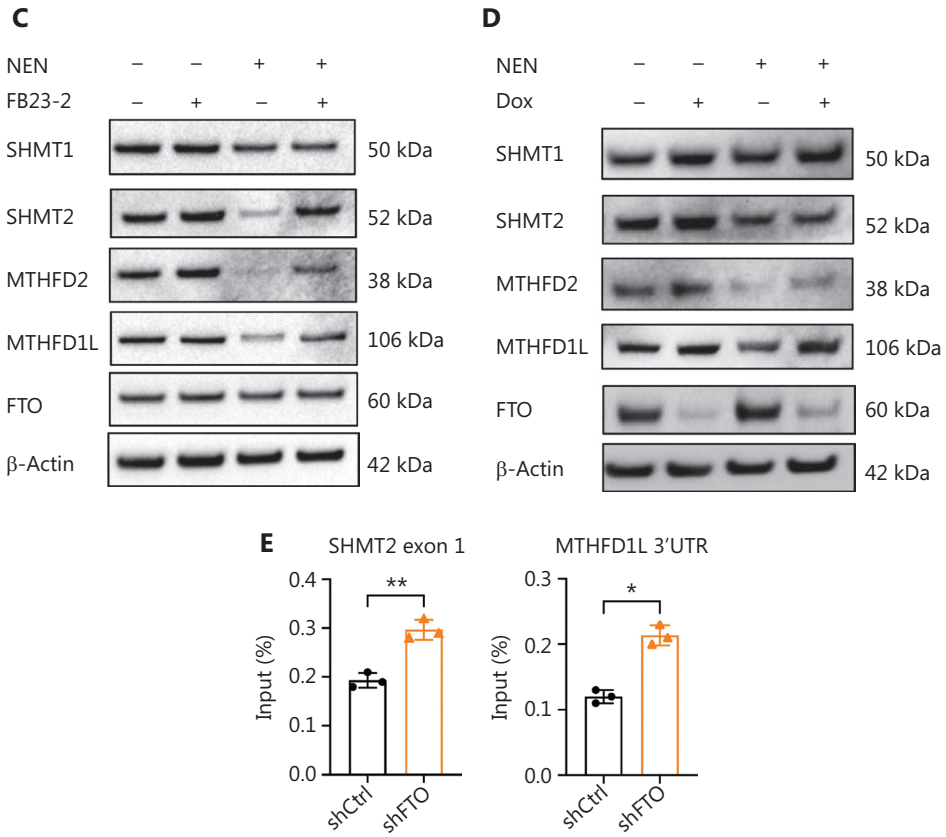

Figure 3 Mitochondrial uncoupling downregulates mitochondrial serine catabolic pathway (MSCP) enzyme expression through FTO. (A) Heatmap showing the expression of RNA-binding proteins in breast cancer and normal tissues. (B) Box plots depicting the average level (transcripts per million) of FTO or ALKBH5 expression in normal tissue and different subtypes of breast cancer. (C) Immunoblot analysis of SCP enzymes in 4175-LM2 cells treated with DMSO control or NEN (1 μM) with or without the FTO inhibitor, FB23-2 (5 μM), for 48 h. (D) Immunoblot analysis of SCP enzymes in 4175-LM2 cells with doxycycline (Dox)-induced FTO knockdown (72 h) and NEN (1 μM) treatment for 48 h. (E) Gene-specific m^{6}A qPCR analysis in *SHMT2* exon I and *MTHFD1L* 3′UTR in 4175-LM2 shCtrl and shFTO cells after m^{6}A IP (MeRIP). Data are presented as the mean ± SEM, n = 3. Statistical significance was determined using an unpaired two-tailed Student's t-test (*P < 0.05, **P < 0.01).

burden (**Figure 6C**). The incidence of lung metastasis was 100% in the control and NEN-treatment groups. No significant changes in mouse body weight were observed (**Figure S4D**). These results suggested that mitochondrial uncoupling represents a promising strategy for targeting metastatic breast cancer.

Discussion

One century ago Otto H. Warburg discovered the phenomenon now known as the Warburg effect, which was proposed as a prime cause of cancer. The Warburg effect reflects impaired mitochondrial respiration, leading to reduced ETC activity, resulting in complex I inhibition and a decreased NAD$^+$:NADH ratio[52]. This reductive stress is central to the key metabolic changes during tumorigenesis[53] and other metabolic diseases[54]. For example, a low NAD$^+$:NADH ratio promotes lactate production (the Warburg effect *per se*[55]) in addition to inhibiting the forward tricarboxylic acid (TCA) cycle, while enhancing reductive carboxylation[56]. In addition, the low NAD$^+$:NADH ratio favors the promiscuous production of L-2-hydroxyglutarate (L-2-HG), which inhibits α-ketoglutarate–dependent dioxygenases, ultimately driving HIF activation and histone hypermethylation, processes that favor tumor progression[46,47]. Furthermore, D-2-HG can be generated from α-KG *via* an NADH-dependent reduction catalyzed by PHGDH[48]. Therefore, reversing the Warburg effect and the associated metabolic reprogramming in cancer requires reactivation of the ETC to restore the NAD$^+$:NADH ratio.

The frequent upregulation of the serine biosynthetic enzyme, phosphoglycerate dehydrogenase (PHGDH)[57-59], combined with the limited availability of serine in the tumor microenvironment[60,61], indicates that tumor cells have an

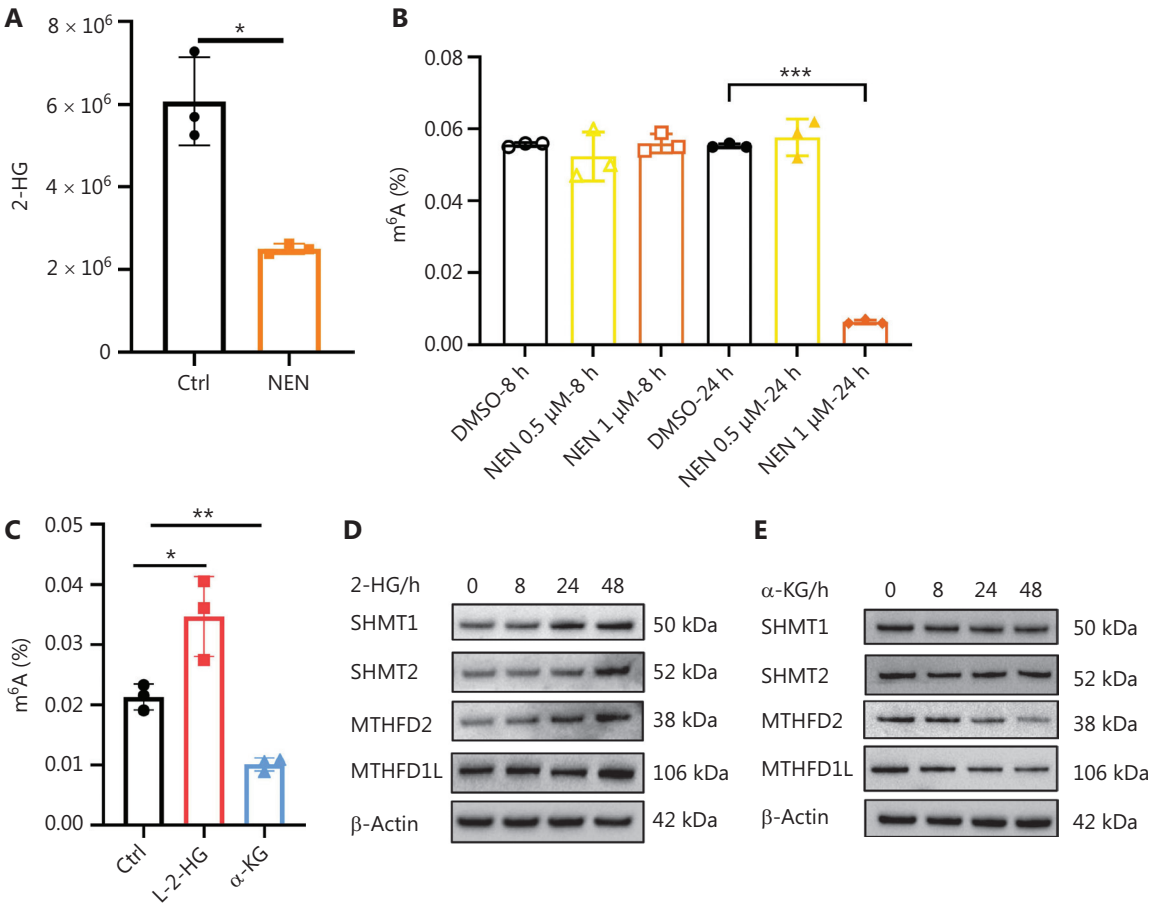

Figure 4 Reduction of 2-HG mediates the effects of mitochondrial uncoupling on MSCP enzyme regulation. (A) 4175-LM2 cells were treated with 1 μM NEN for 24 h. 2-HG levels were determined using LC-MS. (B) 4175-LM2 cells were treated with 0.5 μM or 1 μM NEN for 8 or 24 h and m^6A levels were determined using an EpiQuik m^6A RNA Methylation Quantification Kit. (C) 4175-LM2 cells were treated with 0.2 mM octyl-(S)-2-HG or 2.5 mM dimethyl α-KG for 24 h and m^6A levels were determined with an EpiQuik m^6A RNA Methylation Quantification Kit. For (A)–(C), data represent the mean ± SD, $n = 3$, $^*P < 0.05$, $^{**}P < 0.01$, $^{***}P < 0.001$ by two-tailed Student's *t*-test. (D and E) Immunoblot analysis of SCP enzymes in 4175-LM2 cells treated with 0.2 mM octyl-(S)-2-HG or 2.5 mM dimethyl α-KG for the time indicated.

elevated demand for serine to sustain metabolic and biosynthetic needs compared to normal cells. The MSCP serves as a key compensatory mechanism to sustain NAD(P)H production in tumor cells with impaired ETC activity[5,8,12]. Acute ETC inhibition suppresses oxidative flux through the TCA cycle but MSCP flux remains active and becomes a major catabolic route for NADH production[14]. This finding is because MTHFD2, a key enzyme in MSCP, has a much lower K_m for NAD^+ than NAD^+-dependent dehydrogenases in the TCA cycle, allowing MTHFD2 to function even when NAD^+ levels are low. In contrast, SHMT2, another critical MSCP enzyme, is a direct transcriptional target of HIF-1 and is upregulated under hypoxia, especially in Myc-amplified cancers[12]. These features position MSCP as a universally upregulated metabolic pathway in cancer, conferring a fitness advantage to cancer cells under conditions of respiratory inhibition[11,12]. However, despite the importance of this finding, there is currently no effective therapeutic strategy to selectively inhibit this pathway for cancer treatment.

In addition to the upregulation of MSCP, other major metabolic hallmarks of cancer, such as the Warburg effect, reductive carboxylation, and 2-HG production, are also closely associated with ETC inhibition[53,62,63]. Recently, we demonstrated that mitochondrial uncoupling is an effective strategy for activating the ETC and increasing the NAD^+:NADH ratio[53,62,64]. Mitochondrial uncouplers are a class of drugs that dissipate the proton gradient across the inner mitochondrial membrane, thereby stimulating the ETC and increasing respiration. By restoring mitochondrial respiration, mitochondrial uncoupling not only inhibits the Warburg effect[23] but also reduces 2-HG levels, leading to HIF inactivation, global epigenetic remodeling, and induction of cell differentiation[22].

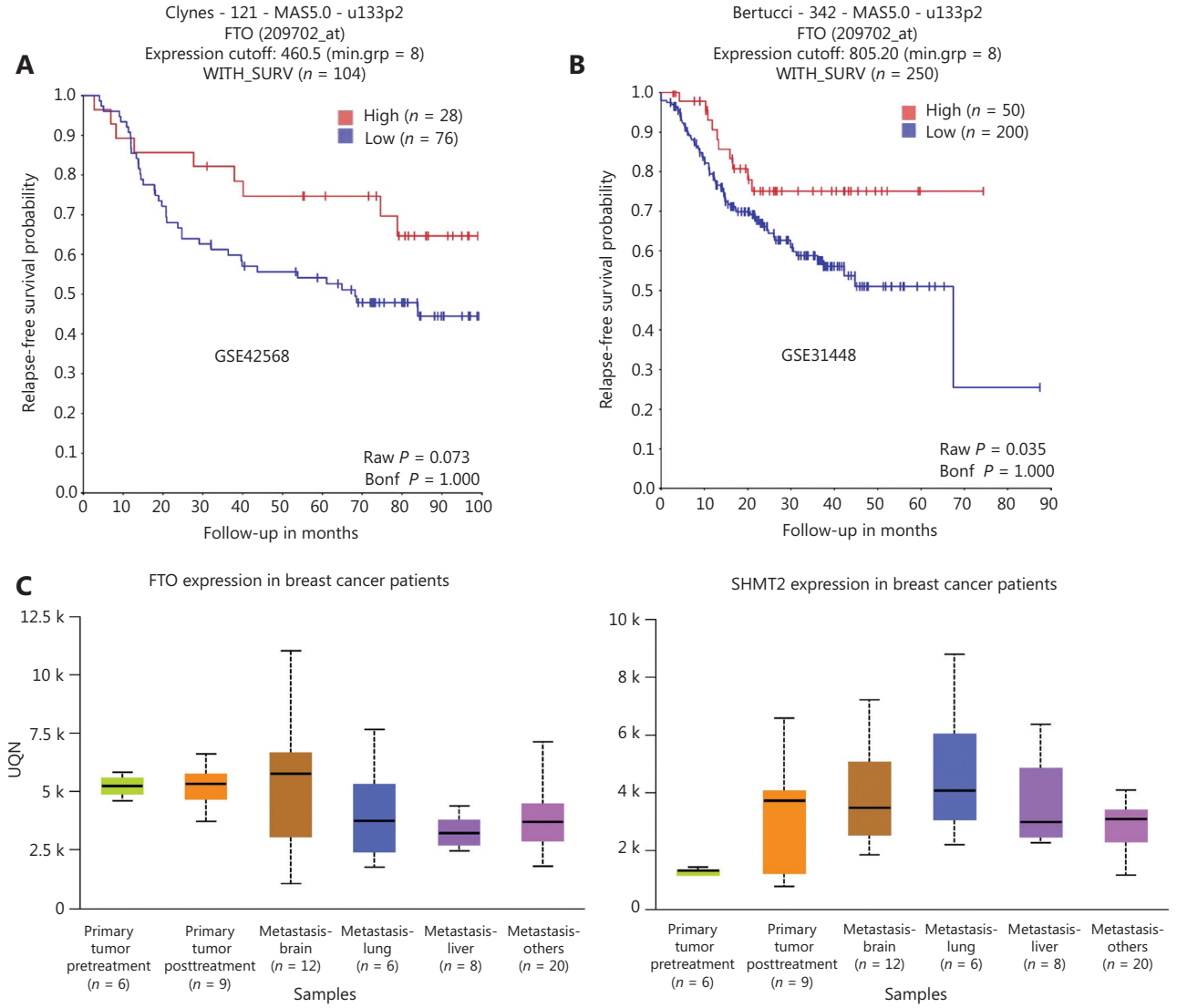

Figure 5 High FTO expression is associated with increased relapse-free survival in breast cancer patients. (A) and (B) Kaplan–Meier survival curves comparing FTO-high and -low patients in two patient cohorts (GSE42568 and GSE31448). (C) Levels of FTO and SHMT2 RNA expression across different stages of breast cancer. UQN; Upper Quartile Normalization.

Furthermore, mitochondrial uncoupling suppresses reductive carboxylation under hypoxic conditions and in VHL-deficient ccRCC cells[65].

Mitochondrial uncoupling was shown herein to inhibit another metabolic hallmark of cancer (activation of the MSCP). Acute treatment with mitochondrial uncouplers significantly reduced the serine-to-glycine conversion, likely by reactivating other NAD^+-dependent pathways, such as the TCA cycle[22]. Moreover, prolonged uncoupler treatment led to a marked downregulation of the three key MSCP enzymes (SHMT2, MTHFD2, and MTHFD1L). Interestingly, this downregulation does not occur at the transcriptional level but instead involves FTO-dependent post-transcriptional regulation.

Recent studies have revealed that FTO downregulation promotes tumor growth and epithelial–mesenchymal transition (EMT) in breast and prostate cancers, suggesting that FTO acts as a tumor suppressor[66]. As an α-KG-dependent dioxygenase, FTO is inhibited by 2-HG, which contributes to tumor metastasis and pro-tumoral macrophage polarization[67]. Both D-2-HG and L-2-HG are present in breast cancer tissues and cell lines, with L-2-HG being the dominant form in ER-negative cancer cells[45]. While tumors harboring mIDH can be targeted with mIDH inhibitors, there are currently no targeted therapies to specifically lower 2-HG that is generated under hypoxia or other conditions of ETC inhibition, when NADH levels are high[46,47].

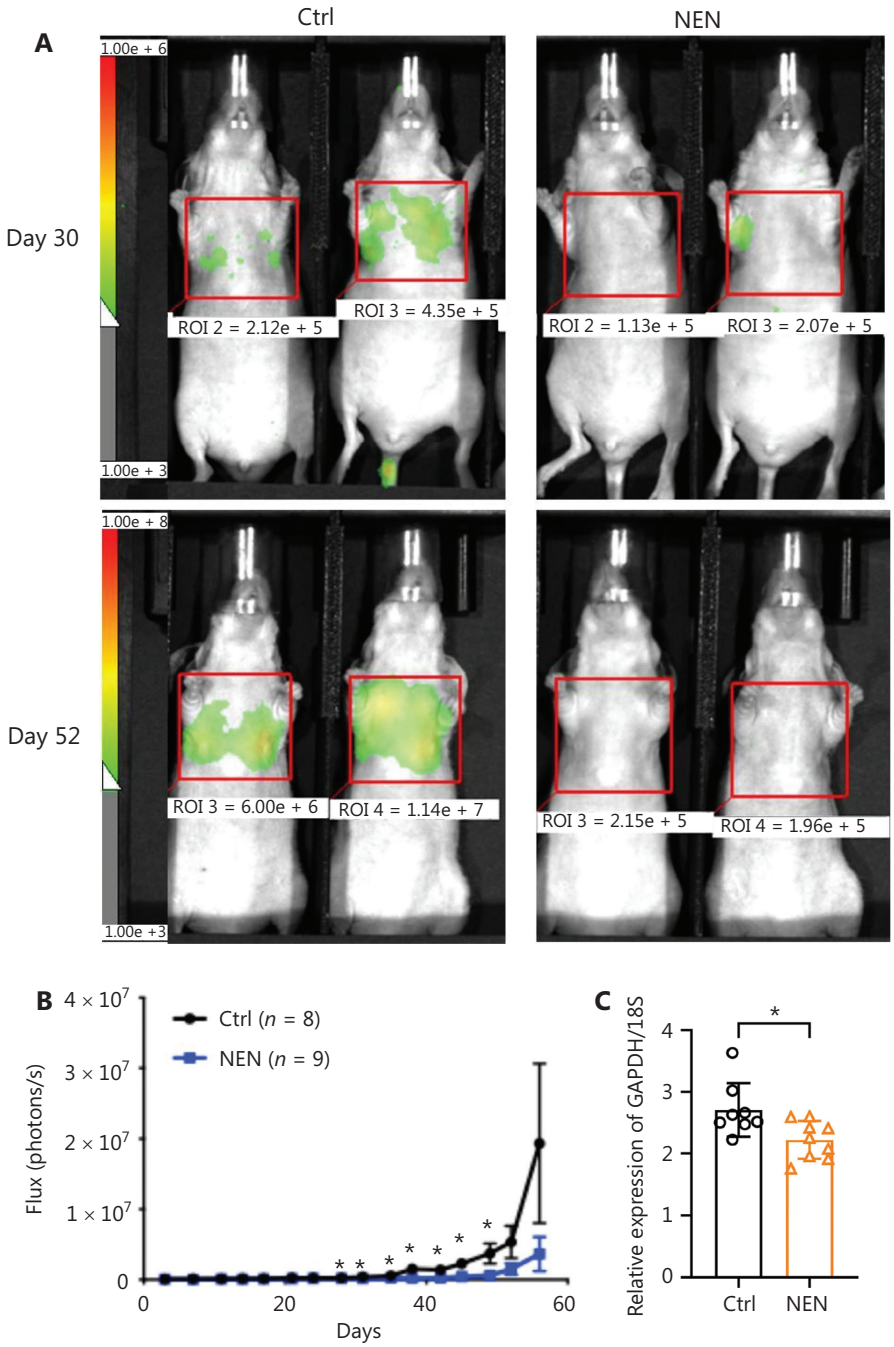

Figure 6 Mitochondrial uncoupling inhibits breast cancer metastasis. (A) Representative images of tumor burden and (B) quantification of luminescence signal in the lungs of control diet- or NEN diet-fed mice injected with 4175-LM cells (mean ± SEM; *P < 0.05 by two-tailed Student's t-test, ctrl: n = 8; NEN: n = 9). (C) Quantification of human tumor burden in mouse lungs from control and NEN-treated groups. Human tumor content was measured by qPCR using the ratio of human GAPDH-to-human and mouse 18S. Data are presented as the mean ± SEM. Ctrl: n = 8; NEN: n = 9.

We recently reported that mitochondrial uncoupling could inhibit 2-HG production under hypoxic conditions, suggesting that mitochondrial uncouplers hold therapeutic potential for lowering 2-HG in mIDH-negative cancers[22]. Building on our previous findings that uncoupling lowers 2-HG, induces CpG island promoter demethylation, and promotes cell differentiation in neuroblastomas, we have now demonstrated that mitochondrial uncoupling reduces 2-HG levels in a

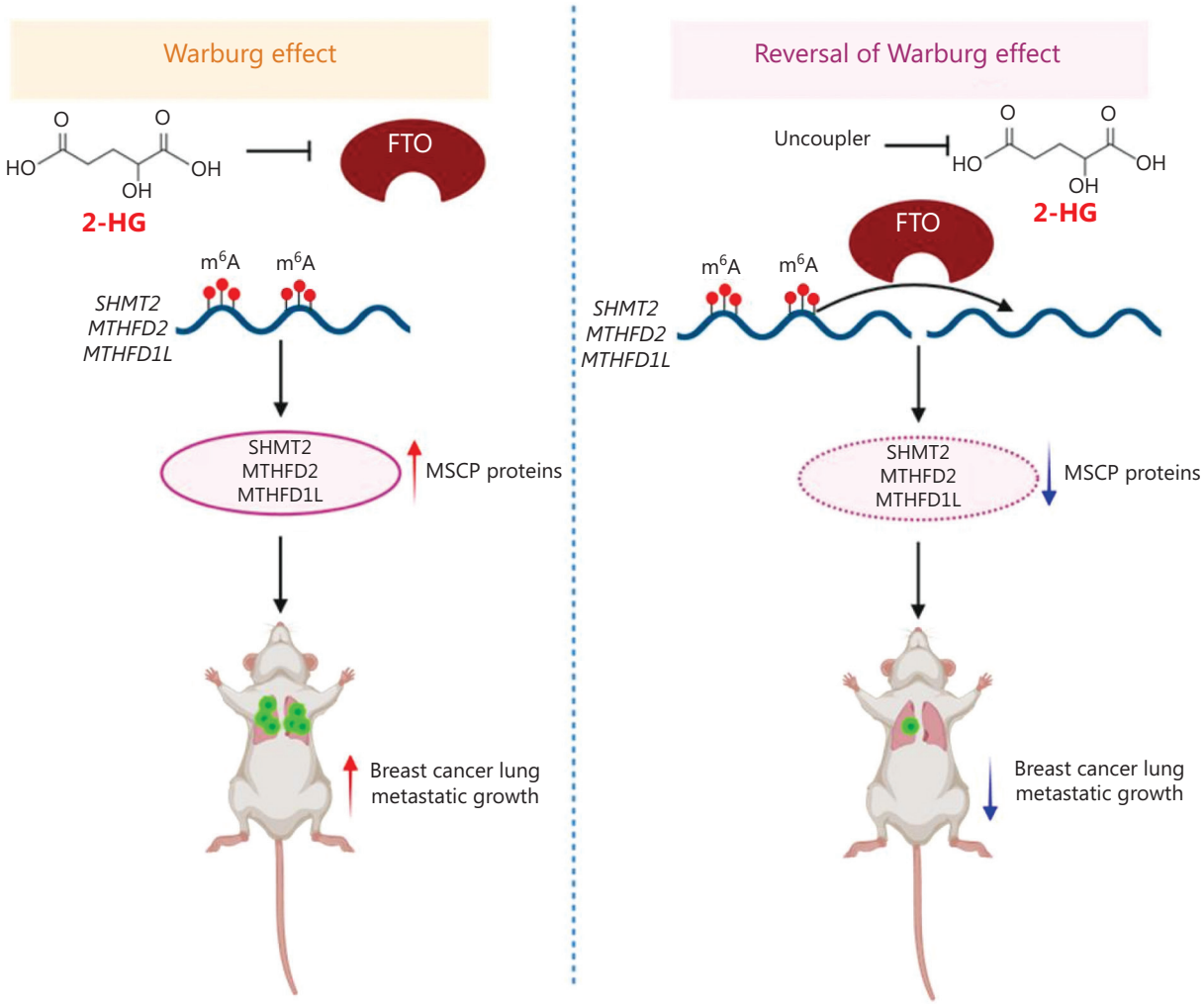

Figure 7 Mitochondrial uncoupling inhibits serine catabolism through FTO activation in metastatic breast cancer. Left: The m^{6}A RNA demethylase, FTO, utilizes α-KG as a substrate. Under the Warburg effect, the reduced NAD$^+$:NADH ratio leads to conversion of α-KG to 2-HG. 2-HG, which is structurally similar to α-KG, acts as a competitive inhibitor of FTO. This inhibition results in the accumulation of m^{6}A on target RNAs, including target RNAs encoding the MSCP pathway enzymes, SHMT2, MTHFD2, and MTHFD1L. The resulting upregulation of these enzymes, which are essential for *de novo* purine biosynthesis, thereby fulfills the metabolic demands of metastatic breast cancer cell proliferation. Right: Mitochondrial uncouplers, a class of compounds that dissipate the proton gradient across the inner mitochondrial membrane, can activate electron transport chain activity and alleviate reductive stress. This activation of the electron transport chain restores the NAD$^+$:NADH ratio, reverses the Warburg effect, and lowers 2-HG levels. Consequently, FTO activity is recovered, leading to decreased m^{6}A methylation on MSCP gene transcripts, reduced expression of the corresponding enzymes, and suppressed metastasis. α-KG, α-ketoglutarate; 2-HG, 2-hydroxyglutarate; m^{6}A, N^6-methyladenosine; FTO, fat mass and obesity-associated protein; SHMT2, serine hydroxymethyltransferase 2; MTHFD2, methylenetetrahydrofolate dehydrogenase 2; MTHFD1L, methylenetetrahydrofolate dehydrogenase 1-like.

similar manner, resulting in decreased m^{6}A RNA methylation in breast cancer cells (**Figure 7**). Notably, downregulation of MSCP enzymes following uncoupling can be rescued by FTO inhibition, confirming the central role of FTO and m^{6}A methylation in regulating MSCP activity and metabolic adaptation.

Despite the excellent safety profile and FDA approval as an anti-parasitic agent, niclosamide has demonstrated limited efficacy in oncology clinical trials[64]. The initial rationale for this failure centered on poor oral bioavailability[68]. However, the lack of efficacy in colon cancer trials is unlikely due to bioavailability issues because oral administration should result in high local drug concentrations directly within the gastrointestinal tract, the target site for these cancers. Recent discoveries have implicated a narrow therapeutic window as a major contributing factor[69,70]. Therefore, future efforts to develop effective cancer therapies should focus on structurally modifying

niclosamide to widen its therapeutic index[70] or investigating other mitochondrial uncouplers, such as BAM15, that inherently possess a broader dosing window[69].

Conclusions

Together with our previous findings, the results herein revealed that metabolic reprogramming in cancer is not a collection of isolated events but rather a systemic response to mitochondrial dysfunction and ETC inhibition[53,62-64]. Therefore, activating ETC through mitochondrial uncoupling offers a unique therapeutic strategy to reverse multiple layers of cancer-associated metabolic reprogramming and target the central dogma at both the epigenetic and epi-transcriptomic levels. Tumorigenesis represents a global cellular transformation, one that may only be effectively counteracted by metabolic therapy capable of reversing all these global changes.

Acknowledgments

We thank Dr. Joan Massagué (Memorial Sloan-Kettering Cancer Center) for providing 4175-LM2 and MDA-MB-468 cells and Dr. Laura Attardi (Stanford University) for providing MiaPaCa-2 and Panc-1 cells.

Grant support

This work was supported by the Stanford Maternal and Child Health Research Institute Faculty Scholar Award (2020), the American Cancer Society Research Scholar Grant (Grant No. RSG-20–036–01), and the Agilent University Relations SIRA program (Grant ID #4792) to J.Y.

Conflict of interest statement

The authors declare no conflicts of interest.

Declaration of generative AI and AI-assisted technologies in the writing process

During the preparation of this work the authors used ChatGPT to enhance the language quality. After using this tool, the authors reviewed and edited the content as needed and take full responsibility for the content of the publication.

Author contributions

Conceived and designed the analysis: Jiangbin Ye, Albert M. Li, Xin Jin, Erinn B. Rankin.

Collected the data: Xin Jin, Albert M. Li, Man Zhao, Haowen Jiang, Yiren Xiao, Michaela Yip, Stavros Melemenidis, Jiangbin Ye.

Contributed data or analysis tools: Yanan Yang, Cathyrin Simmermaker, Daniel J. Cuthbertson.

Performed the analysis: Scott Jackson, Meng-Ning Zhou, Subarna Sinha.

Wrote the paper: Jiangbin Ye, Xin Jin, Albert M. Li, Erinn B. Rankin, Man Zhao.

Data availability statement

The data generated in this study are available upon request from the corresponding author.

References

1. Li AM, Ye J. The PHGDH enigma: do cancer cells only need serine or also a redox modulator? Cancer Lett. 2020; 476: 97-105.
2. Li AM, Ye J. Reprogramming of serine, glycine and one-carbon metabolism in cancer. Biochim Biophys Acta Mol Basis Dis. 2020; 1866: 165841.
3. Locasale JW. Serine, glycine and one-carbon units: cancer metabolism in full circle. Nat Rev Cancer. 2013; 13: 572-83.
4. Yang M, Vousden KH. Serine and one-carbon metabolism in cancer. Nat Rev Cancer. 2016; 16: 650-62.
5. Fan J, Ye J, Kamphorst JJ, Shlomi T, Thompson CB, Rabinowitz JD. Quantitative flux analysis reveals folate-dependent NADPH production. Nature. 2014; 510: 298-302.
6. Ducker GS, Rabinowitz JD. One-carbon metabolism in health and disease. Cell Metab. 2017; 25: 27-42.
7. Zhu J, Berisa M, Schwörer S, Qin W, Cross JR, Thompson CB. Transsulfuration activity can support cell growth upon extracellular cysteine limitation. Cell Metab. 2019; 30: 865-76.e5.
8. Ducker GS, Chen L, Morscher RJ, Ghergurovich JM, Esposito M, Teng X, et al. Reversal of cytosolic one-carbon flux compensates for loss of the mitochondrial folate pathway. Cell Metab. 2016; 23: 1140-53.
9. Tibbetts AS, Appling DR. Compartmentalization of mammalian folate-mediated one-carbon metabolism. Annu Rev Nutr. 2010; 30: 57-81.
10. Chen L, Zhang Z, Hoshino A, Zheng HD, Morley M, Arany Z, et al. NADPH production by the oxidative pentose-phosphate pathway supports folate metabolism. Nat Metab. 2019; 1: 404-15.
11. Nilsson R, Jain M, Madhusudhan N, Sheppard NG, Strittmatter L, Kampf C, et al. Metabolic enzyme expression highlights a key role for MTHFD2 and the mitochondrial folate pathway in cancer. Nat Commun. 2014; 5: 3128.
12. Ye J, Fan J, Venneti S, Wan YW, Pawel BR, Zhang J, et al. Serine catabolism regulates mitochondrial redox control during hypoxia. Cancer Discov. 2014; 4: 1406-17.
13. Li AM, Ducker GS, Li Y, Seoane JA, Xiao Y, Melemenidis S, et al. Metabolic profiling reveals a dependency of human metastatic

breast cancer on mitochondrial serine and one-carbon unit metabolism. Mol Cancer Res. 2020; 18: 599-611.
14. Yang L, Garcia Canaveras JC, Chen Z, Wang L, Liang L, Jang C, et al. Serine catabolism feeds NADH when respiration is impaired. Cell Metab. 2020; 31: 809-21.e6.
15. Minn AJ, Gupta GP, Siegel PM, Bos PD, Shu W, Giri DD, et al. Genes that mediate breast cancer metastasis to lung. Nature. 2005; 436: 518-24.
16. Xiao Y, Thakkar KN, Zhao H, Broughton J, Li Y, Seoane JA, et al. The m^{6}A RNA demethylase FTO is a HIF-independent synthetic lethal partner with the VHL tumor suppressor. Proc Natl Acad Sci U S A. 2020; 117: 21441-9.
17. Einstein JM, Perelis M, Chaim IA, Meena JK, Nussbacher JK, Tankka AT, et al. Inhibition of YTHDF2 triggers proteotoxic cell death in MYC-driven breast cancer. Mol Cell. 2021; 81: 3048-64.e9.
18. Clarke C, Madden SF, Doolan P, Aherne ST, Joyce H, O'Driscoll L, et al. Correlating transcriptional networks to breast cancer survival: a large-scale coexpression analysis. Carcinogenesis. 2013; 34: 2300-8.
19. Sabatier R, Finetti P, Adelaide J, Guille A, Borg JP, Chaffanet M, et al. Down-regulation of ECRG4, a candidate tumor suppressor gene, in human breast cancer. PLoS One. 2011; 6: e27656.
20. Alasadi A, Chen M, Swapna GVT, Tao H, Guo J, Collantes J, et al. Effect of mitochondrial uncouplers niclosamide ethanolamine (NEN) and oxyclozanide on hepatic metastasis of colon cancer. Cell Death Dis. 2018; 9: 215.
21. Kenwood BM, Weaver JL, Bajwa A, Poon IK, Byrne FL, Murrow BA, et al. Identification of a novel mitochondrial uncoupler that does not depolarize the plasma membrane. Mol Metab. 2014; 3: 114-23.
22. Jiang H, Greathouse RL, Tiche SJ, Zhao M, He B, Li Y, et al. Mitochondrial uncoupling induces epigenome remodeling and promotes differentiation in neuroblastoma. Cancer Res. 2023; 83: 181-94.
23. Jiang H, Tiche SJ, He CJ, Liu J, Bian F, Jedoui M, et al. Restoring mitochondrial quantity and quality to reverse the Warburg effect and drive neuroblastoma differentiation. Proc Natl Acad Sci U S A. 2025; 122: e2502483122.
24. Nikiforov MA, Chandriani S, O'Connell B, Petrenko O, Kotenko I, Beavis A, et al. A functional screen for Myc-responsive genes reveals serine hydroxymethyltransferase, a major source of the one-carbon unit for cell metabolism. Mol Cell Biol. 2002; 22: 5793-800.
25. Haggerty TJ, Zeller KI, Osthus RC, Wonsey DR, Dang CV. A strategy for identifying transcription factor binding sites reveals two classes of genomic c-Myc target sites. Proc Natl Acad Sci U S A. 2003; 100: 5313-8.
26. Xuan J, Chen L, Chen Z, Pang J, Huang J, Lin J, et al. RMBase v3.0: decode the landscape, mechanisms and functions of RNA modifications. Nucleic Acids Res. 2024; 52: D273-D84.
27. Wang P, Doxtader KA, Nam Y. Structural basis for cooperative function of Mettl3 and Mettl14 methyltransferases. Mol Cell. 2016; 63: 306-17.
28. Wang X, Feng J, Xue Y, Guan Z, Zhang D, Liu Z, et al. Structural basis of N^6-adenosine methylation by the METTL3-METTL14 complex. Nature. 2016; 534: 575-8.
29. Liu J, Yue Y, Han D, Wang X, Fu Y, Zhang L, et al. A METTL3-METTL14 complex mediates mammalian nuclear RNA *N*^{6}-adenosine methylation. Nat Chem Biol. 2014; 10: 93-5.
30. Ping XL, Sun BF, Wang L, Xiao W, Yang X, Wang WJ, et al. Mammalian WTAP is a regulatory subunit of the RNA N6-methyladenosine methyltransferase. Cell Res. 2014; 24: 177-89.
31. Wen J, Lv R, Ma H, Shen H, He C, Wang J, et al. Zc3h13 regulates nuclear RNA m^{6}A methylation and mouse embryonic stem cell self-renewal. Mol Cell. 2018; 69: 1028-38.e6.
32. Pendleton KE, Chen B, Liu K, Hunter OV, Xie Y, Tu BP, et al. The U6 snRNA m^{6}A methyltransferase METTL16 regulates SAM synthetase intron retention. Cell. 2017; 169: 824-35.e14.
33. Doxtader KA, Wang P, Scarborough AM, Seo D, Conrad NK, Nam Y. Structural basis for regulation of METTL16, an S-adenosylmethionine homeostasis factor. Mol Cell. 2018; 71: 1001-11.e4.
34. Mendel M, Chen KM, Homolka D, Gos P, Pandey RR, McCarthy AA, et al. Methylation of structured RNA by the m^{6}A writer METTL16 is essential for mouse embryonic development. Mol Cell. 2018; 71: 986-1000.e11.
35. Jia G, Fu Y, Zhao X, Dai Q, Zheng G, Yang Y, et al. *N*6-methyladenosine in nuclear RNA is a major substrate of the obesity-associated FTO. Nat Chem Biol. 2011; 7: 885-7.
36. Huang H, Weng H, Sun W, Qin X, Shi H, Wu H, et al. Recognition of RNA *N*^{6}-methyladenosine by IGF2BP proteins enhances mRNA stability and translation. Nat Cell Biol. 2018; 20: 285-95.
37. Cerneckis J, Ming GL, Song H, He C, Shi Y. The rise of epitranscriptomics: recent developments and future directions. Trends Pharmacol Sci. 2024; 45: 24-38.
38. Roundtree IA, Evans ME, Pan T, He C. Dynamic RNA modifications in gene expression regulation. Cell. 2017; 169: 1187-200.
39. Pomaville MM, He C. Advances in targeting RNA modifications for anticancer therapy. Trends Cancer. 2023; 9: 528-42.
40. Zhao M, Zhang D, Jiang H, Kuganesan N, Natarajan S, Pu L, et al. The RNA demethylase FTO promotes glutamine metabolism in clear cell renal cell carcinoma through the regulation of SLC1A5. Sci Adv. 2025; 11: eadv2417.
41. Zheng G, Dahl JA, Niu Y, Fedorcsak P, Huang CM, Li CJ, et al. ALKBH5 is a mammalian RNA demethylase that impacts RNA metabolism and mouse fertility. Mol Cell. 2013; 49: 18-29.
42. Su R, Dong L, Li C, Nachtergaele S, Wunderlich M, Qing Y, et al. R-2HG exhibits anti-tumor activity by targeting FTO/m^{6}A/MYC/CEBPA signaling. Cell. 2018; 172: 90-105.e23.
43. Kundu A, Brinkley GJ, Nam H, Karki S, Kirkman R, Pandit M, et al. l-2-Hydroxyglutarate remodeling of the epigenome and epitranscriptome creates a metabolic vulnerability in kidney cancer models. J Clin Invest. 2024; 134: e171294.

44. Terunuma A, Putluri N, Mishra P, Mathe EA, Dorsey TH, Yi M, et al. MYC-driven accumulation of 2-hydroxyglutarate is associated with breast cancer prognosis. J Clin Invest. 2014; 124: 398-412.
45. Kusi M, Zand M, Lin LL, Chen M, Lopez A, Lin CL, et al. 2-Hydroxyglutarate destabilizes chromatin regulatory landscape and lineage fidelity to promote cellular heterogeneity. Cell Rep. 2022; 38: 110220.
46. Intlekofer AM, Dematteo RG, Venneti S, Finley LW, Lu C, Judkins AR, et al. Hypoxia induces production of L-2-hydroxyglutarate. Cell Metab. 2015; 22: 304-11.
47. Oldham WM, Clish CB, Yang Y, Loscalzo J. Hypoxia-mediated increases in L-2-hydroxyglutarate coordinate the metabolic response to reductive stress. Cell Metab. 2015; 22: 291-303.
48. Fan J, Teng X, Liu L, Mattaini KR, Looper RE, Vander Heiden MG, et al. Human phosphoglycerate dehydrogenase produces the oncometabolite D-2-hydroxyglutarate. ACS Chem Biol. 2015; 10: 510-6.
49. Ye D, Guan KL, Xiong Y. Metabolism, activity, and targeting of D- and L-2-hydroxyglutarates. Trends Cancer. 2018; 4: 151-65.
50. Karthikeyan SK, Chandrashekar DS, Sahai S, Shrestha S, Aneja R, Singh R, et al. MammOnc-DB, an integrative breast cancer data analysis platform for target discovery. NPJ Breast Cancer. 2025; 11: 35.
51. Tao H, Zhang Y, Zeng X, Shulman GI, Jin S. Niclosamide ethanolamine-induced mild mitochondrial uncoupling improves diabetic symptoms in mice. Nat Med. 2014; 20: 1263-9.
52. Zhao Y, Wang A, Zou Y, Su N, Loscalzo J, Yang Y. *In vivo* monitoring of cellular energy metabolism using SoNar, a highly responsive sensor for NAD^+/NADH redox state. Nat Protoc. 2016; 11: 1345-59.
53. Bagatell R, Park JR, Acharya S, Aldrink J, Allison J, Alva E, et al. Neuroblastoma, version 2.2024, NCCN Clinical Practice Guidelines in Oncology. J Natl Compr Canc Netw. 2024; 22: 413-33.
54. Yang R, Guo Z, Li B. NADH reductive stress drives metabolic reprogramming. Trends Cell Biol. 2025. DOI: 10.1016/j.tcb.2025.07.005.
55. Zhao Y, Hu Q, Cheng F, Su N, Wang A, Zou Y, et al. SoNar, a highly responsive NAD^+/NADH sensor, allows high-throughput metabolic screening of anti-tumor agents. Cell Metab. 2015; 21: 777-89.
56. Gaude E, Schmidt C, Gammage PA, Dugourd A, Blacker T, Chew SP, et al. NADH shuttling couples cytosolic reductive carboxylation of glutamine with glycolysis in cells with mitochondrial dysfunction. Mol Cell. 2018; 69: 581-93.e7.
57. Possemato R, Marks KM, Shaul YD, Pacold ME, Kim D, Birsoy K, et al. Functional genomics reveal that the serine synthesis pathway is essential in breast cancer. Nature. 2011; 476: 346-50.
58. Locasale JW, Grassian AR, Melman T, Lyssiotis CA, Mattaini KR, Bass AJ, et al. Phosphoglycerate dehydrogenase diverts glycolytic flux and contributes to oncogenesis. Nat Genet. 2011; 43: 869-74.
59. Ye J, Mancuso A, Tong X, Ward PS, Fan J, Rabinowitz JD, et al. Pyruvate kinase M2 promotes de novo serine synthesis to sustain mTORC1 activity and cell proliferation. Proc Natl Acad Sci U S A. 2012; 109: 6904-9.
60. Kamphorst JJ, Nofal M, Commisso C, Hackett SR, Lu W, Grabocka E, et al. Human pancreatic cancer tumors are nutrient poor and tumor cells actively scavenge extracellular protein. Cancer Res. 2015; 75: 544-53.
61. Pan M, Reid MA, Lowman XH, Kulkarni RP, Tran TQ, Liu X, et al. Regional glutamine deficiency in tumours promotes dedifferentiation through inhibition of histone demethylation. Nat Cell Biol. 2016; 18: 1090-101.
62. Jiang H, Jedoui M, Ye J. The Warburg effect drives dedifferentiation through epigenetic reprogramming. Cancer Biol Med. 2023; 20: 891-7.
63. Jiang H, Ye J. The Warburg effect: the hacked mitochondrial-nuclear communication in cancer. Semin Cancer Biol. 2025; 112: 93-111.
64. Jiang H, Li AM, Ye J. The magic bullet: niclosamide. Front Oncol. 2022; 12: 1004978.
65. Jiang H, He CJ, Li AM, He B, Li Y, Zhou MN, et al. Mitochondrial uncoupling inhibits reductive carboxylation in cancer cells. Mol Cancer Res. 2023; 21: 1010-6.
66. Jeschke J, Collignon E, Al Wardi C, Krayem M, Bizet M, Jia Y, et al. Downregulation of the FTO m^6A RNA demethylase promotes EMT-mediated progression of epithelial tumors and sensitivity to Wnt inhibitors. Nat Cancer. 2021; 2: 611-28.
67. Zhang S, Zhang N, Wan T, He Y, Hao J, Liu Y, et al. Oncometabolite D-2HG drives tumor metastasis and protumoral macrophage polarization by targeting FTO/m^6A/ANGPTL4/integrin axis in triple-negative breast cancer. J Exp Clin Cancer Res. 2025; 44: 41.
68. Schweizer MT, Haugk K, McKiernan JS, Gulati R, Cheng HH, Maes JL, et al. A phase I study of niclosamide in combination with enzalutamide in men with castration-resistant prostate cancer. PLoS One. 2018; 13: e0198389.
69. Shah DP, Vancuylenburg CS, Olzomer EM, Chen SY, Grams RJ, Beretta M, et al. Diverse actions of 15 structurally unrelated mitochondrial uncouplers in cells and mice. Mol Metab. 2025; 99: 102204.
70. Jiang H, Macorano A, Xing E, Jedoui M, Mohammed S, Lee V, et al. Discovery of niclosamide analogs with potent mitochondrial uncoupling activity and reduced mitochondrial inhibition–associated toxicity. ACS Med Chem Lett. 2025: DOI: 10.1021/acsmedchemlett.5c00439.

Cite this article as: Jin X, Li AM, Zhao M, Jiang H, Xiao Y, Yip M, et al. Mitochondrial uncoupling inhibits serine catabolism *via* FTO activation in metastatic breast cancer. Cancer Biol Med. 2026; 23: 1303-1319. doi: 10.20892/j.issn.2095-3941.2025.0444